Volume 12
Number 3
21 January 2024
Pages 739–1134

# Journal of Materials Chemistry C

Materials for optical, magnetic and electronic devices

rsc.li/materials-c

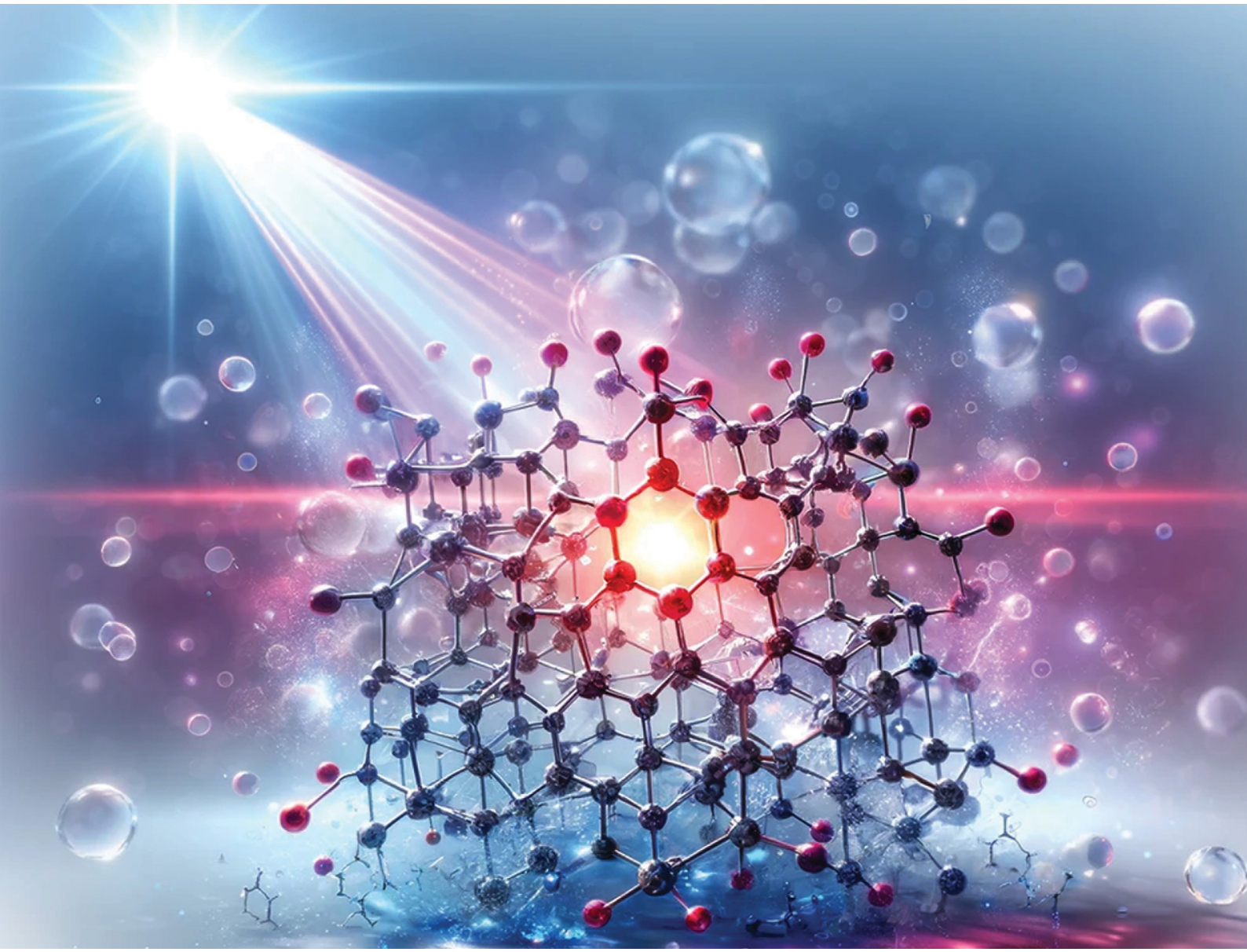

ISSN 2050-7526

ROYAL SOCIETY OF CHEMISTRY

**PAPER**

Kexin Wang, Jiwei Wang *et al.*
Solvent-induced luminescence behavior of Ce/Eu@Gd-MOF for ratiometric detection of $D_2O$ in $H_2O$

Journal of Materials Chemistry C

ROYAL SOCIETY OF CHEMISTRY

PAPER

View Article Online
View Journal | View Issue



Cite this: J. Mater. Chem. C, 2024, 12, 868

# Solvent-induced luminescence behavior of Ce/Eu@Gd-MOF for ratiometric detection of $D_2O$ in $H_2O$†

Xiaoxuan Fan,[a] Zhiqiang Guo,[a] Xiaokun Wen,[b] Wen Liu,[a] Baijie Guan,[a] Feifei Yin,[a] Xia Hong,[b] Tianya Tan,[a] Kexin Wang*[a] and Jiwei Wang*[a]

The solvent environment has a significant impact on the luminescence performance of Ln-MOFs, but the related research studies are still limited. In this work, a Ln-MOF using 1,3,5-benzenetricarboxylic acid as ligands and $Ce^{3+}$/$Eu^{3+}$ as luminescence centers was prepared. The photoluminescence behaviors of Ce/Eu@Gd-MOFs were studied in $H_2O$ and $D_2O$. The emission intensity of the Ce/Eu@Gd-MOFs dispersed in $D_2O$ is improved by 711.19% compared to that dispersed in $H_2O$. After excluding the effects of solvent reabsorption and pH, the difference in vibrational frequencies of the functional groups in $H_2O$ and $D_2O$ is considered to be the main reason for the enhanced luminescence. Deuterated hydroxyl groups have lower vibrational frequencies than hydroxyl groups, resulting in effective weakening of nonradiative transitions. Vibrational coupling occurs between the deuterated hydroxyl groups, $H_3BTC$ ligands and $Ce^{3+}$, because of the proximity of the vibrational frequency of the deuterated hydroxyl groups and the energy level gaps between $H_3BTC$ ligands and $Ce^{3+}$. This facilitates the energy transfer through vibration–vibration interaction in non-radiative processes. The enhancement in luminescence and energy transfer efficiency of Ce/Eu@Gd-MOFs in $D_2O$ is attributed to the synergistic effect of the above mechanisms. This solvent-induced luminescence behavior of Ce/Eu@Gd-MOFs holds potential as an approach for detecting $D_2O$ in $H_2O$. The detection sensitivity reaches 0.001%. This study contributes to the understanding of the Ln-MOF luminescence and offers insights into its practical applications.

Received 13th November 2023,
Accepted 30th November 2023

DOI: 10.1039/d3tc04154a

rsc.li/materials-c



## 1. Introduction

Lanthanide metal–organic frameworks (Ln-MOFs) have emerged as a fascinating class of framework materials in recent years, attracting considerable attention.[1–5] The integration of lanthanide ions and organic ligands confers outstanding optical properties to Ln-MOFs, rendering them with extensive applications in biochemical sensing, nonlinear optics, and white light-emitting diodes.[6–8] The solvent environment is one of the most crucial factors affecting the luminescence performance of Ln-MOFs in applications. Ln-MOFs are dispersed in solution accompanied by a framework breathing effect.[9] The porous structure of Ln-MOFs leads to direct interactions between solvent molecules and the lanthanide ions. This results in alterations of intermolecular interactions in Ln-MOFs, causing Ln-MOFs to exhibit distinct properties in the solvent environment compared to their solid-state counterparts.[10–12] However, there is still a lack of comprehensive knowledge regarding the influence of solvents on the luminescence of Ln-MOFs. The intricate differences including chemical reactivity, dispersibility, hydrogen bonding, pH, and reabsorption among different solvent molecules pose challenges.[13] The systematic study for the influence of solvents on the Ln-MOFs luminescence performance is of great significance for customizing luminescence functionalities and advancing their practical applications.

$D_2O$ is an important isotope of $H_2O$, exhibiting a similar modular structure.[14–16] It possesses irreplaceable application value in chemical analysis, nuclear energy production, spectroscopic characterization and bioanalysis.[17–19] The similarity in the physical and chemical properties renders $D_2O$ and $H_2O$ highly suitable candidates for exploring solvent-induced luminescence behavior, minimizing the influence of factors such as solvent viscosity, chemical reactivity, and dispersibility.[20–22] From another perspective, the investigation of the luminescence behavior of Ln-MOFs in $H_2O$ and $D_2O$ also presents an opportunity to provide a rapid and convenient approach for detecting $D_2O$ content in $H_2O$.

[a] College of Physics, Liaoning University, Shenyang, 110036, China
[b] Key Laboratory of UV-Emitting Materials and Technology (Northeast Normal University), Ministry of Education, Changchun, 130024, China

† Electronic supplementary information (ESI) available. See DOI: https://doi.org/10.1039/d3tc04154a

Herein, we prepared a Ln-MOF using a one-pot solvothermal method, with 1,3,5-benzenetricarboxylic acid ($H_3BTC$) as ligands and $Ce^{3+}$/$Eu^{3+}$ as luminescence centers. The doping concentrations of $Ce^{3+}$ and $Eu^{3+}$ in MOFs help in optimizing the photoluminescence (PL) performance. The PL properties of Ce/Eu@Gd-MOFs in $H_2O$ and $D_2O$ were investigated systematically. The impacts of solvent reabsorption, pH value, vibration frequency of solvent molecules and energy gap on luminescence processes, particularly on the energy transfer process, were discussed in detail. The energy transfer efficiencies of $Ce^{3+}$ and $Eu^{3+}$ in $H_2O$ and $D_2O$ were calculated based on the time-resolved spectra. The detection of $D_2O$ content in $H_2O$ was achieved based on the Ce/Eu@Gd-MOFs showing application potential.

## 2. Experimental section

### 2.1 Materials and chemicals

$CH_3COONa$, $Ce(NO_3)_3{\cdot}6H_2O$, $GdCl_3{\cdot}6H_2O$, $EuCl_3{\cdot}6H_2O$, 1,3,5-benzenetricarboxylic acid ($H_3BTC$) and *N*,*N*-dimethylformamide (DMF) were purchased from Macklin Reagent Co., Ltd. $D_2O$ was purchased from Aladdin Reagent Co., Ltd. Deionized water was used in all aqueous solutions. All chemicals were analytical grade reagents and used directly without further purification.

### 2.2 Preparation of MOFs

A series of Ce@Gd-MOFs, Eu@Gd-MOFs, and Ce/Eu@Gd-MOFs were synthesized by a solvothermal method. An example of preparing $Ce_{0.01}/Eu_{0.002}@Gd_{0.987}$-MOFs: the starting materials $Ce(NO_3)_3{\cdot}6H_2O$ (0.0043 g), $GdCl_3{\cdot}6H_2O$ (0.3608 g), $EuCl_3{\cdot}6H_2O$ (0.0008 g) and $H_3BTC$ (0.1050 g) were weighed according to the stoichiometric ratio. Then, the ingredients were dissolved in DMF (100 mL). The solution was sonicated for 10 min at room temperature. The component $CH_3COONa$ (0.1360 g) was added to the solution and sonication continued for 30 min. The mixed solution was transferred to an autoclave and kept at 120 °C for 24 h. Finally, a white product was obtained, washed by DMF, ethanol and deionized water and dried at 60 °C for 24 h.

### 2.3 Characterization

The morphology of the MOFs was characterized by scanning electron microscopy (SEM, JEOL, JSM-7800F Prime) energy dispersive X-ray (EDX) spectroscopy. The crystal phase of all the phosphor samples was identified by using X-ray powder diffraction (XRD) analysis with a Rigaku D/MAX-RB diffractometer (Tongda TD-3500 automatic X-ray diffractometer system). Fourier transform infrared (FTIR) transmittance spectra of the MOFs were characterized by using a Nicolet IS10 spectrometer under a liquid nitrogen environment. The emission and excitation spectra were measured by using a fluorescence spectrometer (Hitachi, F-7000). Time-resolved fluorescence spectra of the MOFs were recorded by using a transient optical testing system (Quanta Master 400, Photon Technology International).

## 3. Results and discussion

### 3.1 Phase identification

The MOF is composed of lanthanide ions ($Gd^{3+}$, $Ce^{3+}$ and $Eu^{3+}$) and $H_3BTC$ ligands by coordination. The unit of the MOF consists of a seven-coordinate $Gd^{3+}$ cation, a coordinated water molecule, and a $H_3BTC$ ligand (Fig. 1a). The metal sites of $Gd^{3+}$ can be occupied by $Ce^{3+}$ and $Eu^{3+}$ due to similar ionic radii and valence states. The coordination environment of the metal ions and $H_3BTC$ is shown in Fig. 1b. Fig. 1c reveals that the metal ions are connected through carboxylic bridges to form a one-dimensional helical chain. These chains are further linked with $H_3BTC$ ligands to construct a three-dimensional framework structure (Fig. 1d). Fig. 1e displays the XRD patterns of Ce@Gd-MOFs, Eu@Gd-MOFs and Ce/Eu@Gd-MOFs. The XRD patterns are matched well with the diffraction peaks reported in the literature.[23–25] This indicates that the doping of rare earth ions has no impact on the formation of the crystal structure of the MOFs. Fig. 1f is the FTIR spectrum of Ce/Eu@Gd-MOFs and $H_3BTC$. The spectrum of precursor $H_3BTC$ is provided for comparison. The broad band centered at 3397 $cm^{-1}$ is owing to the stretching vibration of hydroxyl groups. In the Ce/Eu@Gd-MOFs spectrum, the peaks at 1617 $cm^{-1}$, 1550 $cm^{-1}$, 1440 $cm^{-1}$ and 1375 $cm^{-1}$ are assigned to the antisymmetric and symmetric stretching mode vibrations of carboxyl groups. They exhibit a shift compared to those in the spectrum of $H_3BTC$. This originated from the coordination between $H_3BTC$ ligands and metal ions. The SEM image of Ce/Eu@Gd-MOFs is shown in Fig. 1g. The MOFs exhibit a rod-like morphology. Fig. 1h presents the element distribution of Ce/Eu@Gd-MOFs. The elements of O, C, Ce, Eu and Gd are observed in the EDX analysis. This indicates that $Ce^{3+}$, $Eu^{3+}$ and $Gd^{3+}$ are successfully formed MOFs with $H_3BTC$ ligands.

### 3.2 Luminescence properties

Fig. 2a presents the emission spectra of Ce@Gd-MOFs, Eu@Gd-MOFs and Ce/Eu@Gd-MOFs. The MOFs all have a broad

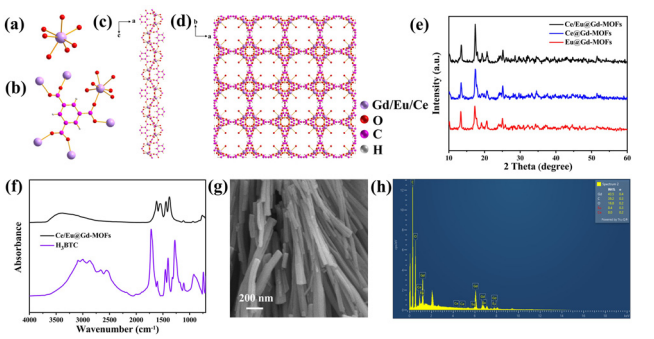


Fig. 1 (a) The coordination environments of $Gd^{3+}$, $Eu^{3+}$ and $Ce^{3+}$ in Ln-MOF. (b) Coordination mode of the $BTC^{3-}$ ligand and the coordination environments of $Gd^{3+}$, $Eu^{3+}$ and $Ce^{3+}$. (c) 1D metal–organic framework along the *b* axis. (d) 3D metal–organic framework along the *c* axis. (e) XRD patterns of Ce@Gd-MOFs, Eu@Gd-MOFs, and Ce/Eu@Gd-MOFs. (f) FTIR spectra of benzene-1,3,5-tricarboxylic acid and Ce/Eu@Gd-MOFs samples. (g) SEM image of Ce/Eu@Gd-MOFs. (h) Energy dispersive X-ray (EDX) spectrum of Ce/Eu@Gd-MOFs.

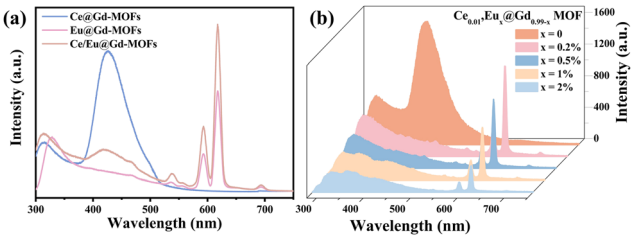


Fig. 2 (a) Emission spectra of Ce@Gd-MOFs, Eu@Gd-MOFs and Ce/Eu@Gd-MOFs, and (b) emission spectra of Ce/Eu@Gd-MOFs ($\lambda_{ex}$ = 260 nm).

emission band in the range of 315–345 nm, assigned to the π–π* transition of the ligands.[26] The Ce@Gd-MOFs show blue emission under 260 nm excitation. The broad emission band centered at 425 nm is ascribed to parity-allowed 5d → 4f transitions of $Ce^{3+}$.[27] The emission spectrum of Eu@Gd-MOFs shows peaks at 595 nm, 613 nm, and 690 nm. They arise from $^5D_0 \rightarrow {}^7F_J$ ($J$ = 1, 2, and 4) transitions of $Eu^{3+}$.[28,29] The co-doped Ce/Eu@Gd-MOFs exhibit both characteristic emissions of $Ce^{3+}$ and $Eu^{3+}$. In order to optimize the PL performance, the doping concentration of $Eu^{3+}$ was regulated.[30,31] The emission spectra of $Eu_x@Gd_{1-x}$-MOFs ($x$ = 0, 0.002, 0.005, 0.01, and 0.02) and $Ce_{0.01}/Eu_x@Gd_{0.99-x}$-MOFs ($x$ = 0.002, 0.005, 0.01, and 0.02) are recorded in Fig. S1 (ESI†). The emission intensity of Ce/Eu@Gd-MOFs increases by 763.33% compared to the MOFs with only $Eu^{3+}$ doping. The emission spectra of $Ce_{0.01}/Eu_x@Gd_{0.99-x}$-MOFs ($x$ = 0, 0.002, 0.005, 0.01, and 0.02) under 260 nm excitation are shown in Fig. 2b. It was clearly found that the emission intensity of $Ce^{3+}$ decreased with $Eu^{3+}$ concentration increasing. The $Eu^{3+}$ optimum doping concentration is $x$ = 0.002. This implies that energy transfer occurs between $Eu^{3+}$ and $Ce^{3+}$ in the MOFs. $Ce^{3+}$ is excited from the ground state 4f to the excited state 5d. One part of the energy of the excited $Ce^{3+}$ returns to the ground state, while the rest of the excited $Ce^{3+}$ returns to the excited state ($^5D_0$) of $Eu^{3+}$.

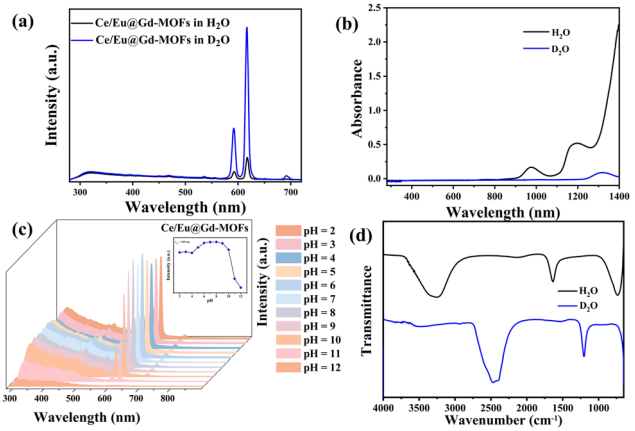


Fig. 3 (a) Emission spectra of Ce/Eu@Gd-MOFs dispersed in $H_2O$ and $D_2O$. (b) UV-Vis-NIR absorption spectra of $H_2O$ and $D_2O$. (c) Emission spectra of Ce/Eu@Gd-MOFs in $H_2O$ (pH = 2–12). The inset expresses luminescence intensity at 260 nm. (d) FTIR spectra of $H_2O$ and $D_2O$.

The solvent environment plays a crucial role in the luminescence behavior and energy transfer processes of rare earth ions.[13,21,32] The PL properties of Ce/Eu@Gd-MOFs dispersed in $H_2O$ and $D_2O$ are shown in Fig. 3a. The $Eu^{3+}$ emission intensity at 617 nm improves by 711.19% when the MOFs are dispersed in $D_2O$ compared to that in $H_2O$ (Fig. S2, ESI†). The reasons for the solvent-induced luminescence behavior require further investigation. The UV-Vis-NIR absorption spectra of $H_2O$ and $D_2O$ were characterized to study the effect of solvent molecules on the emission and excitation of Ce/Eu@Gd-MOFs. As shown in Fig. 3b, $H_2O$ has two absorption bands centered at 977 nm and 1181 nm, respectively. $D_2O$ presents a weak absorption band at 1322 nm. This indicates that $H_2O$ and $D_2O$ have no effect on the emission (425 nm and 617 nm) and excitation (260 nm) of Ce/Eu@Gd-MOFs. The differences on the pH values of the solvent may cause protonation or deprotonation. The emission spectra of Ce/Eu@Gd-MOFs dispersed in $H_2O$ (pH value from 2 to 12) are recorded in Fig. 3c. The emission intensity of Ce/Eu@Gd-MOFs exhibits a trend of initially increasing and then decreasing with pH value from 2 to 12. When the pH value is between 6 and 8, the emission intensity reaches its maximum and remains nearly constant. This indicates that the difference of pH value between $H_2O$ (pH = 6.4–7.0) and $D_2O$ (pH = 7.5) is not the main factor for the luminescence variation. FTIR spectra of $H_2O$ and $D_2O$ are shown in Fig. 3d. $H_2O$ has characteristic absorption bands positioned at 3325 $cm^{-1}$, 1637 $cm^{-1}$, and 736 $cm^{-1}$. These absorption bands correspond to the stretching vibration, variable angle vibration, and oscillation vibration of hydroxyl groups. The absorption bands of deuterated hydroxyl groups in $D_2O$ show a blue shift, demonstrating that the deuterated hydroxyl groups have lower vibrational frequencies. The luminescence behavior and energy transfer processes of $Eu^{3+}$ and $Ce^{3+}$ can be affected by the vibrational frequencies of solvent molecules. According to Hook's Law:

$$v = \frac{1}{2}\pi\sqrt{\frac{k}{u}}$$

$$u = m_1 \cdot m_2/(m_1 + m_2)$$

where $v$ is the chemical bond vibrational frequency, $k$ is the telescopic force constant, and $m$ is the relative atomic mass. The $k_{O-H} \approx k_{O-D} \approx 7.8$, $u_{O-H} < u_{O-D}$. The vibrational frequencies of hydroxyl groups are greater than those of the deuterated hydroxyl groups. Low vibrational frequencies of the deuterated hydroxyl groups can help in avoiding vibrational relaxation and reduce the probability of non-radiative transitions.[33,34] The impact of solvent molecule vibration frequency on the energy transfer process in MOFs needs further exploration.

### 3.3 Effect of solvent on energy transfer in MOFs

Fig. 4 illustrates the energy transfer between $H_3BTC$ ligands, $Ce^{3+}$ and $Eu^{3+}$ in the PL process of Ce/Eu@Gd-MOFs. The $H_3BTC$ ligands absorb photons *via* the antenna effect and are excited from the singlet state ($S_1$, 36978 $cm^{-1}$) to the triplet

 

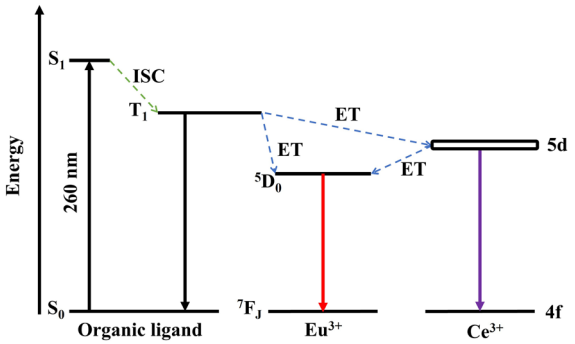


Fig. 4 The energy level diagram and possible energy transfer schemes among $H_3BTC$ ligands, $Ce^{3+}$ and $Eu^{3+}$.

state ($T_1$, 26491 $cm^{-1}$) through intersystem crossing (ISC) according to the Reinhold empirical rule.[1,35–37] The triplet state of $H_3BTC$ ligand transfers energy to the 5d excited state of $Ce^{3+}$ and $^5D_0$ of $Eu^{3+}$ *via* a non-radiative process.[38–42] The energy gap between the $T_1$ of $H_3BTC$ ligands, $Ce^{3+}$ and $Eu^{3+}$ is 2453 $cm^{-1}$ and 9685 $cm^{-1}$, respectively. This means that the sensitization effect of $H_3BTC$ ligands on $Ce^{3+}$ is significantly higher than that on $Eu^{3+}$. The excited state of $Ce^{3+}$ further transfers energy to $Eu^{3+}$, leading to the emission of $Eu^{3+}$ from $^5D_0$ to $^7F_J$.

Time-resolved PL decay curves were tested to further study the excited-state radiative relaxation and energy transfer processes of Ce/Eu@Gd-MOFs in $H_2O$ and $D_2O$ (Fig. 5). All of the decay traces of the Ce/Eu@Gd-MOFs are well fitted with a biexponential function. As the concentration of $Eu^{3+}$ increases, the decay times for both $Ce^{3+}$ and $Eu^{3+}$ ions decrease. This stems from the effective energy transfer from the sensitizer ($Ce^{3+}$) to the activator ($Eu^{3+}$), leading to a decrease in the decay times as the concentration of the activator increases (Table 1).[26] Both the lifetimes of $Ce^{3+}$ and $Eu^{3+}$ are extended when the dispersing solvent of Ce/Eu@Gd-MOFs is changed from $H_2O$ to

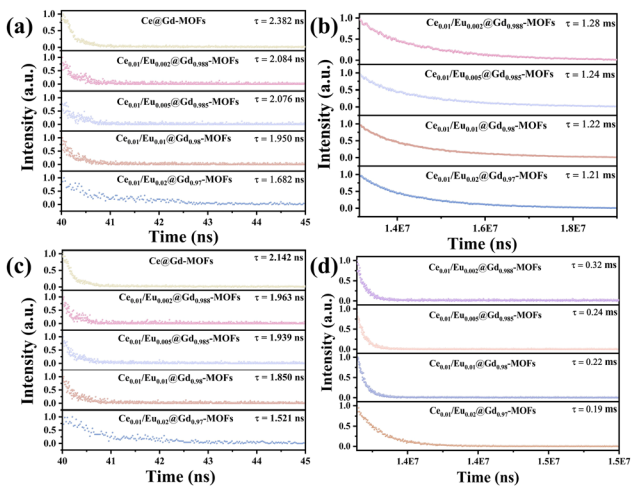


Fig. 5 Time-resolved PL decay curves of Ce/Eu@Gd-MOFs (a) $Ce^{3+}$ in $D_2O$, (b) $Eu^{3+}$ in $D_2O$, (c) $Ce^{3+}$ in $H_2O$, and (d) $Eu^{3+}$ in $H_2O$. The excitation wavelength is 280 nm. The monitored wavelength is 394 nm for $Ce^{3+}$ and 617 nm for the decay curve of $Eu^{3+}$.

$D_2O$. This arises from the low vibrational frequency of deuterated hydroxyl groups in $D_2O$ weakening vibrational relaxation.[43] Moreover, the stretching vibration frequency of deuterated hydroxyl groups (2469 $cm^{-1}$) is close to the energy gap between $Ce^{3+}$ and the $H_3BTC$ ligands ($T_1$-5d, 2453 $cm^{-1}$). This implies the vibrational coupling occurring between the excited state of the ligands and $Ce^{3+}$, resulting in increased probability of vibrational relaxation. This vibrational relaxation tends to hinder radiative transition processes, but it is beneficial for vibration–vibration interaction of energy transfers between the $H_3BTC$ ligands and $Ce^{3+}$. The luminescence of Ce/Eu@Gd-MOFs is consequently enhanced.

The energy transfer efficiencies of $Ce^{3+}$ and $Eu^{3+}$ in $H_2O$ and $D_2O$ were calculated by the following formula:[44,45]

$$\eta = 1 - \frac{\tau}{\tau_0}$$

$\eta$ represents the energy transfer efficiency between $Ce^{3+}$ and $Eu^{3+}$ in $H_2O$ or $D_2O$, $\tau$ and $\tau_0$ stand for the luminescence lifetimes of $Ce^{3+}$ with doped and undoped $Eu^{3+}$ in MOFs dispersed in $H_2O$ or $D_2O$. As the concentration of impurity $Eu^{3+}$ increases, the energy transfer efficiencies in $H_2O$ and $D_2O$ both gradually improve (Fig. S3, ESI†). The energy transfer efficiency in $H_2O$ is 28.97%, and in $D_2O$ is 29.32% (Table 1). This indicates that the decreased vibration frequency of deuterated hydroxyl groups reduces non-radiative transitions during the luminescence process. The decreased electron migration rate among $Eu^{3+}$ and $Ce^{3+}$ consequently leads to an increase in energy transfer efficiency.

### 3.4 $D_2O$ detection

The distinctive PL behaviors in $H_2O$ and $D_2O$ of Ce/Eu@Gd-MOFs can be utilized for detecting $D_2O$ in $H_2O$. The emission intensity of the ligands at 316 nm has no significant changes in both $H_2O$ and $D_2O$. It can serve as a reference for achieving self-calibration in ratio detection. The emission intensity of $Eu^{3+}$ at 617 nm rises significantly with the increase in the content of $D_2O$ in $H_2O$ from 0% to 100% (Fig. 6a). The ratio of the emission intensities at 617 nm ($F_{617\ nm}$) and 316 nm ($F_{316\ nm}$) shows the expected linear relationship with the proportion of $D_2O$ in $H_2O$. (Fig. 6b). The limit of detection (LOD) is calculated as 0.001%. This result suggests that the Ce/Eu@Gd-MOFs are capable of serving as a ratiometric luminescence probe for the sensitive detection of $D_2O$ in $H_2O$. The selectivity of $D_2O$ detection has been evaluated by comparing the emission intensities at 316 nm and 617 nm of the Ce/Eu@Gd-MOFs dispersed in the presence of common species. The interfering species include methanol, ethanol, acetone, $Na^+$, $K^+$, $Ca^{2+}$, $Mg^{2+}$ and $Zn^{2+}$. The results are presented in Fig. S4 (ESI†). They demonstrate that the Ce/Eu@Gd-MOFs have an acceptable selectivity in $D_2O$ detection.

## 4. Conclusions

In summary, Ce/Eu@Gd-MOFs were synthesized using $H_3BTC$ as a ligand and $Ce^{3+}$/$Eu^{3+}$ as luminescence centers. The

Table 1 $Ce^{3+}$ and $Eu^{3+}$ lifetimes in $D_2O$ and $H_2O$ depending on $Eu^{3+}$ concentration

| $Eu^{3+}$ concentration (mol) | $Ce^{3+}$ lifetime (ns) in $D_2O$ | $Eu^{3+}$ lifetime (ms) in $D_2O$ | $Ce^{3+}$ lifetime (ns) in $H_2O$ | $Eu^{3+}$ lifetime (ms) in $H_2O$ |
|---|---|---|---|---|
| 0 | 2.382 | | 2.142 | |
| 0.002 | 2.084 | 1.28 | 1.962 | 0.32 |
| 0.005 | 2.076 | 1.24 | 1.939 | 0.24 |
| 0.01 | 1.950 | 1.22 | 1.850 | 0.22 |
| 0.02 | 1.682 | 1.21 | 1.521 | 0.19 |
| Max energy transfer efficiency ($\eta$) | 29.32% | | 28.97% | |

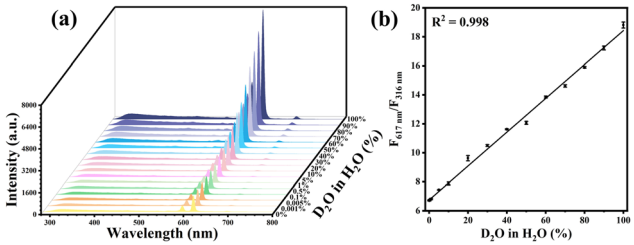


Fig. 6 (a) Luminescence spectra of Ce/Eu@Gd-MOFs with $D_2O$ content ranging from 0% to 100%. (b) Correlation between $D_2O$ content and $F_{617\ nm}/F_{316\ nm}$.

differentiated luminescence behaviors of Ce/Eu@Gd-MOFs in $H_2O$ and $D_2O$ are attributed to the differences in vibrational frequencies between hydroxyl groups and deuterated hydroxyl groups. The PL enhancement of Ce/Eu@Gd-MOFs dispersed in $D_2O$ is attributed to the combination of low vibrational frequency and matching with the energy level gaps of deuterated hydroxyl groups. The energy transfer efficiency of $Ce^{3+}$ and $Eu^{3+}$ in the MOF increases from 28.97% to 29.32% as the solvent changes from $H_2O$ to $D_2O$. The Ce/Eu@Gd-MOFs were used as ratiometric luminescence probes for detecting $D_2O$ in $H_2O$. The LOD is calculated as 0.001%. This work is expected to provide guidance for the solvent-involved applications of MOFs in bioimaging, therapies, sensing, solar cells, *etc.*

## Conflicts of interest

There are no conflicts to declare.

## Acknowledgements

This work was supported by the National Natural Science Foundation of China (Grant No. 51972052), the Open Foundation of Key Laboratory for UV-Emitting Materials and Technology of Ministry of Education (Northeast Normal University, No. 135131009), the Doctoral Start-up Foundation and Natural Science Foundation of Liaoning Province (2021-BS-085 and 2021-MS-148), General Project of the Department of Education of Liaoning Province (LJKZ0084), and Shenyang Science and Technology Bureau (22-315-6-06).

## References

1 Y. Zhao and D. Li, *J. Mater. Chem. C*, 2020, **8**, 12739–12754.
2 X. Wang, Y. Jiang, A. Tissot and C. Serre, *Coord. Chem. Rev.*, 2023, **497**, 215454.
3 H. N. Abdelhamid, M. Wilk-Kozubek, A. M. El-Zohry, A. Bermejo Gómez, A. Valiente, B. Martín-Matute, A. V. Mudring and X. Zou, *Microporous Mesoporous Mater.*, 2019, **279**, 400–406.
4 W. Gong, Z. Chen, J. Dong, Y. Liu and Y. Cui, *Chem. Rev.*, 2022, **122**, 9078–9144.
5 X. Y. Liu, W. P. Lustig and J. Li, *ACS Energy Lett.*, 2020, **5**, 2671–2680.
6 J. Dong, D. Zhao, Y. Lu and W.-Y. Sun, *J. Mater. Chem. A*, 2019, **7**, 22744–22767.
7 T. N. Nguyen, F. M. Ebrahim and K. C. Stylianou, *Coord. Chem. Rev.*, 2018, **377**, 259–306.
8 Y. Tang, H. Wu, W. Cao, Y. Cui and G. Qian, *Adv. Opt. Mater.*, 2020, **9**, 2001817.
9 L. Feng, C. Dong, M. Li, L. Li, X. Jiang, R. Gao, R. Wang, L. Zhang, Z. Ning, D. Gao and J. Bi, *J. Hazard. Mater.*, 2020, **388**, 121816.
10 R. Seetharaj, P. V. Vandana, P. Arya and S. Mathew, *Arabian J. Chem.*, 2019, **12**, 295–315.
11 D. S. Choi, D. W. Kim, J. H. Lee, Y. S. Chae, D. W. Kang and C. S. Hong, *ACS Appl. Mater. Interfaces*, 2021, **13**, 38358–38364.
12 S. Song, X. Ma, W. Li, B. Zhang, J. Sun and C. Deng, *Colloids Surf., A*, 2023, **656**, 130350.
13 T. Cong, Y. Ding, S. Xin, X. Hong, H. Zhang and Y. Liu, *Langmuir*, 2016, **32**, 13200–13206.
14 L. Tcelykh, V. Kozhevnikova Khudoleeva, A. Goloveshkin, L. Lepnev, T. Popelensky and V. Utochnikova, *Analyst*, 2020, **145**, 759–763.
15 X. Guo, B. Liu, R. Kuang, W. Gan, L. Huang and J. Wang, *J. Mater. Chem. C*, 2023, **11**, 7611–7618.
16 S. M. Patil, S. K. Gupta, D. Goswami and R. Gupta, *ACS Omega*, 2023, **8**, 32444–32449.
17 W. Lei, N. W. S. Fong, K. L. Jarvis and D. R. McKenzie, *ACS Appl. Mater. Interfaces*, 2021, **13**, 13666–13675.
18 X. Liu, L. Shi, L. Shi, M. Wei, Z. Zhao and W. Min, *Adv. Sci.*, 2022, **9**, 19658–19662.
19 C. Liu, H. Su, M. Guo, P. Zhai, L. Liu and H. Fu, *Sol. Energy Mater. Sol. Cells*, 2022, **245**, 111861.
20 X. Wang, N. M. Liu, Y. F. Zhao, F. Yang, Z. J. Zhu and D. Song, *Int. J. Med. Sci.*, 2022, **19**, 1357–1363.
21 X. Liu, W. Liu, Z. Ju, J. Jiang and W. Liu, *Inorg. Chem.*, 2022, **61**, 19658–19662.
22 S. G. Dunning, A. J. Nuñez, M. D. Moore, A. Steiner, V. M. Lynch, J. L. Sessler, B. J. Holliday and S. M. Humphrey, *Chem*, 2017, **2**, 579–589.

 

23 M. Hu, Y. Shu, A. Kirillov, W. Liu, L. Yang and W. Dou, *ACS Appl. Mater. Interfaces*, 2021, **13**, 7625–7634.
24 X. Yang, X. Lin, Y. Zhao, Y. S. Zhao and D. Yan, *Angew. Chem., Int. Ed.*, 2017, **56**, 7853–7857.
25 Y. Cai, X. Li, K. Wu and X. Yang, *Anal. Chim. Acta*, 2019, **1062**, 78–86.
26 H. Cheng, Q. Sun, S. Wang, Y. Zhang, D. Fan, J. J. Huang and S. Jin, *J. Phys. Chem. C*, 2019, **123**, 30165–30170.
27 V. R. Rao, C. Basavapoornima, S. R. Depuru and C. K. Jayasankar, *J. Non-Cryst. Solids*, 2020, **549**, 120333.
28 X. Zhang, L. Zhou, Q. Pang, J. Shi and M. Gong, *J. Phys. Chem. C*, 2014, **118**, 7591–7598.
29 J. M. Li, R. Li and X. Li, *CrystEngComm*, 2018, **20**, 4962–4972.
30 P. V. Do, T. Ngoc, N. X. Ca, L. D. Thanh, P. T. T. Nga, T. T. C. Thuy and N. V. Nghia, *J. Lumin.*, 2021, **229**, 117660.
31 D. Yue, Y. Huang, L. Zhang, K. Jiang, X. Zhang, Y. Cui, Y. Yu and G. Qian, *J. Mater. Chem. C*, 2018, **6**, 2054–2059.
32 Z. Guo, X. Fan, X. Wen, W. Liu, B. Guan, X. Hong, K. Wang and J. Wang, *Chem. Commun.*, 2023, **59**, 10408.
33 A. Døssing, *Eur. J. Inorg. Chem.*, 2005, 1425–1434.
34 J. D. Einkauf, J. M. Clark, A. Paulive, G. P. Tanner and D. T. de Lill, *Inorg. Chem.*, 2017, **56**, 5544–5552.
35 X. Yang, H. Zou, X. Sun, T. Sun, C. Guo, Y. Fu, C. M. L. Wu, X. Qiao and F. Wang, *Adv. Opt. Mater.*, 2019, **7**, 1900336.
36 A. Kirch, M. Gmelch and S. Reineke, *J. Phys. Chem. Lett.*, 2019, **10**, 310–315.
37 H. Kang, J. Peng, Z. Zhang and W. Zhou, *J. Lumin.*, 2022, **247**, 118904.
38 Z. Li, R. Núñez, M. E. Light, E. Ruiz, F. Teixidor, C. Viñas, D. Ruiz-Molina, C. Roscini and J. G. Planas, *Chem. Mater.*, 2022, **34**, 4795–4808.
39 W. Fan, Y. Cheng, M. Feng, P. Liu, L. Wang, Y. Liu, Q.-E. Cao and L. Y. Zheng, *ACS Appl. Mater. Interfaces*, 2023, **15**, 41977–41991.
40 T. Xia, Z. Shao, X. Yan, M. Liu, L. Yu, Y. Wan, D. Chang, J. Zhang and D. Zhao, *Chem. Commun.*, 2021, **57**, 3143–3146.
41 J. D. Einkauf, T. T. Kelley, B. C. Chan and D. T. de Lill, *Inorg. Chem.*, 2016, **55**, 7920–7927.
42 X. Rao, T. Song, J. Gao, Y. Cui, Y. Yang, C. Wu, B. Chen and G. Qian, *J. Am. Chem. Soc.*, 2013, **135**, 15559–15564.
43 S. Lis, *J. Alloys Compd.*, 2002, **341**, 45–50.
44 X. Fan, X. Sun, C. Liu, W. Tian, M. Li, Y. Luo and C. Wu, *J. Lumin.*, 2022, **242**, 118594.
45 L. L. da Luz, B. F. Lucena Viana, G. C. O. da Silva, C. C. Gatto, A. M. Fontes, M. Malta, I. T. Weber, M. O. Rodrigues and S. A. Júnior, *CrystEngComm*, 2014, **16**, 6914–6918.